Structural Basis of Glutathione Recognition by the Yeast Cadmium Factor 1

Tik Hang Soong[1], Clare F. Hotze[1], Nitesh Kumar Khandelwal[1,2], and Thomas M. Tomasiak[1]

[1]Department of Chemistry and Biochemistry, University of Arizona, Tucson, AZ 85721, USA

[2]Department of Biochemistry and Physics, University of California San Francisco, San Francisco, CA 94158, USA

Correspondence should be addressed to Tomasiak, Thomas M.

Email: tomasiak@arizona.edu

Author Contributions: T.H.S. conducted protein purification, cryo-EM studies, viability assay, data analysis, and manuscript preparation. C.F.H. performed viability assay, data analysis, and manuscript preparation. N.K.K. aided with methodology. T.M.T. conducted in data analysis, funding acquisition, and prepared manuscript.

Competing Interest Statement: No competing interests are declared

Classification: Biological Sciences, Biochemistry

Keywords: ABC transporter, glutathione transporter, glutathione-metal conjugation

Abstract

Transporters from the ABCC family have an essential role in detoxifying electrophilic compounds including metals, drugs, and lipids, often through conjugation with glutathione complexes. The yeast cadmium factor 1 (Ycf1), plays such a role in yeast, and can transport glutathione alone as well as conjugate to toxic heavy metals including Cd^{2+}, Hg^{2+}, and As^{3+}. To understand the complicated pleiotropy of heavy metal substrate binding, we determined the cryo-EM structure of Ycf1 bound to the substrate, oxidized glutathione, and performed cellular survival assays against heavy metals to determine the basis for pleiotropic binding that adapts to different-sized metal complexes. We identify a “flex-pocket” for substrate binding that binds glutathione complexes asymmetrically and flexes to accommodate different size complexes.

Significance Statement

The molecular mechanism by which Ycf1 transports a broad array of substrates that are essential for cellular detoxification and redox homeostasis remains unknown in the field of cellular biology. Here, guided by the novel substrate bound structure of Ycf1, we discovered a bipartite binding mechanism that accommodates substrates of varying sizes while maintaining specificity. Four crucial ionic interactions govern substrate specificity by recognizing ligands with a glutathione moiety, complemented by a sizable pocket on the adjacent side for different glutathione complexes.

Main Text

Introduction

The ATP Binding Cassette (ABC) transporter superfamily evolved as an ancient system to divert small molecule metabolites, drugs, lipids, metals, and toxins to maintain homeostasis (1). Consequently, their activity has ties to pathogenesis, such as the development of drug resistance or immune evasion mechanisms (2). Yeast (*S. cerevisiae)* maintain a wide-ranging assortment of ABC transporters, in particular, the C subfamily of ABC transporters (ABCC transporters) are responsible for transporting xenobiotics or compartmentalizing toxic metabolites to prevent cellular damage, including heavy metals that induce oxidative stress, disrupt protein function, and even cause membrane damage (3-5). ABCC transporters primarily transport substrates that are modified, typically in the form of glutathione (GSH) conjugation to provide a hydrophilic handle for transport and sequester these toxins (6-10). Several ABCC transporters export toxic heavy metals, which are major environmental pollutants that present a significant health risk to both wildlife and humans alike (11). Exposure to some of these heavy metals can result in adverse effects, such as neurotoxicity, nephrotoxicity, genotoxicity, and hepatotoxicity that may have lasting impacts on human health (12).

In the human liver, the multi-drug resistance protein (MRP) 1 and 2 export GSH-conjugated metals into the bile (13, 14). In fungal systems, GSH-conjugated metals are sequestered into the vacuole, where GSH can be hydrolytically released and be exported back into the cytoplasm for GSH regeneration (15-18). Initially discovered in a screen for proteins important for the stress tolerance transcription factor yAP-1 that exert cadmium resistance, Yeast Cadmium Factor 1 (Ycf1) is the most well-characterized ABCC transporter (19). Later studies showed that Ycf1 functions as a vacuolar transporter that protects the cell by sequestering a GSH conjugated cadmium complex into the vacuole (20). This was the first evidence of GSH conjugated heavy metal transport in yeast (21). Subsequent studies had shown that besides cadmium, Ycf1 also exerts resistance against other major environmental toxins including arsenic, mercury, and lead through a similar vacuolar sequestering mechanism (22-25). As such, Ycf1 has been proposed as a bioremediation target and has shown promising results in phytoremediation purposes (26). Besides GSH conjugated substrate, Ycf1 also transports diglutathione (GSSG), the oxidized form of GSH, into the vacuole (27). In this way, Ycf1 functions similarly to the human MRP1 as a phase III pump that not only detoxifies the cytoplasmic space but also regulates redox homeostasis by maintaining a healthy balance of GSH and GSSG (28). Indeed, MRP1 had been shown to functionally replace Ycf1 when expressed in yeast and exhibited comparable functionality when expressed in insect cells (29-31).

Accurate ligand recognition is of paramount importance for transporters to correctly identify their respective substrates. There is very little known about the mechanism by which Ycf1 recognizes metal-GSH complexes and the specificity factors that dictate proper ligand identification. Structure of the substrate-bound MRP1 revealed a bipartite binding pocket that differentially recognize the polar and hydrophobic components of leukotriene C4 (LTC4), a glutathione conjugated leukotriene A4 (32). However, considering that both GSSG and metal-GSH differ from LTC4 greatly in their polarity, it remains unclear if the same recognition mechanism observed in LTC4-bound MRP1 would be conserved in Ycf1. Furthermore, in Ycf1, the degree of GSH conjugation changes depending on the heavy metal. For example, while cadmium conjugation requires only two GSH, arsenic requires three conjugated GSH to stabilize its trivalent oxidative state. As such, it remains unknown how the recognition mechanism may change with the degree of GSH conjugation.

To shed light onto the substrate recognition mechanism that takes place in Ycf1, we have obtained a 3.1Å resolution structure of GSSG-bound Ycf1 by single-particle cryo-electron microscopy (cryo-EM). Our structure reveals a novel inward-facing conformation of the protein with an antisymmetric GSSG found inside the central cavity. Using a cell-based assay guided by our structure, we discovered that Ycf1has a bipartite binding mechanism resembling that of MRP1 with one pocket

responsible for substrate specificity while the other remains flexible to accommodate different ligand sizes. Our findings provide valuable mechanistic insights into the structural components that underlie substrate recognition in Ycf1.

Results

Using single-particle cryo-EM, the GSSG-bound Ycf1 structure was determined to a resolution of 3.1Å. The map was highly detailed with the canonical ABC transporter transmembrane domain (TMD) core that includes TMD1 and TMD2, as well as cytosolic nucleotide binding domains 1 and 2 (NBD1 and 2) clearly shown (**Fig. 1A**). The TMD0, lasso motif, and regulatory domain (R-domain) that are characteristic of the ABCC subfamily were also observed in the map (**Fig.1A**) in an inward-facing conformation.

In the substrate cavity, density not previously observed was modeled with a GSSG structure (**Fig. 1*A-B***). The two halves of the GSH moiety were found to be arranged in an antiparallel arrangement with each half of GSSG binding to different sets of transmembrane (TM) helices. We term the two binding halves the half one (H1) and half two (H2) pockets. One end of the glycyl group points towards the H1 pocket, and the other glycyl group pointing upwards away from the NBDs in the H2 pocket (**Fig. 1C**). The ligand forms interaction with TMs 6, 7, 8, 9, 11, 12, 14, 16, and 17 (**Fig. 1*C-D***).

As expected, GSSG-Ycf1 adopts a similar conformation as previous open inward-facing models. The α-carbon distance between G668 and S1411 were measured at 35.2Å, 35.4Å, and 36.0Å for GSSG-Ycf1, apo Ycf1 (PDBID:7M69), and dephosphorylated Ycf1 (PDBID:8SG4), respectively (**Fig. 1F**) (33, 34). Therefore, unlike MRP1, substrate binding in Ycf1 does not induce dimerization of NBDs for ATP hydrolysis and instead induces a slight widening of the NBDs (32). To further understand how the TMDs may react to pocket occupancy, the binding pocket volume was calculated for each Ycf1 model with their NBDs (605-900, 1250-1515) and R-domain (901-935) removed. Interestingly, the apo (9499Å^3) and dephosphorylated (9465Å^3) states of Ycf1 had very similar pocket volume, whereas the GSSG-bound (11571Å^3) Ycf1 contained the largest pocket volume (**Fig. 1F**). This result corroborates our data on α-carbon alignment of GSSG-Ycf1 TMDs (275-604 & 936-1249) to apo and dephosphorylated Ycf1 that showed a widening of the TMDs by ~1.4Å in both cases.

GSSG is stabilized by a hydrophobic sandwich capped by basic residues

GSSG binds in a highly basic pocket, especially in H1. The half of GSSG that binds in the H1 pocket is nearly identical to that of the glutathione moiety in LTC4 bound to MRP1 (PDBID:5UJA) despite the drastic difference in polarity between the two ligands. Basic residues on TM6, TM16, and TM17 within the H1 pocket interact extensively with the glutamyl and glycyl groups of the GSH moiety. The hydrophobic disulfide bridge connecting H1 and H2 is sandwiched by hydrophobic, aromatic residues on TM11 and TM17 to further stabilize the substrate binding. As for the GSH moiety in the H2 pocket, the glutamyl group interacts with polar residues on TM14 and TM17, but the glycyl group extends into a largely empty space.

Asymmetry in H1 and H2 sites

The H1 binding site is predominantly basic with contacts to GSSG by K294, H297, R1174 and R1228 (**Fig. 2A**). Loss of these interactions confers cadmium susceptibility in growth conditions with $CdCl_2$ (**Fig. 2B**). Despite similarities to the LTC4 binding in MRP1, several key interactions are different. W422, analogous to Y440 in MRP1, is not positioned to hydrogen bond substrate and showed no influence on substrate transport (**Fig. 2A-B**). N1224 corresponds to N1244 in MRP1 that hydrogen bonds to δ-glutamyl carbonyl group of LTC4. Notably, the δ-glutamyl carbonyl group of GSSG in the H1 pocket is rotated nearly opposite to that of LTC4, thus N1224 makes no contacts with the ligand and had no impact on transporter function (**Fig. 2A-B**). Altogether, the four basic residues anchor the carboxylate end of the GSH moiety to stabilize ligand binding in the H1 pocket.

Compared to H1, the H2 pocket sustained fewer and weaker interactions. N1074 and T1222 were observed to hydrogen bond with the glutamyl amine of the GSH moiety inside the H2 binding site (**Fig. 2B**). Although T1222A mutation did compromise substrate transport in Ycf1, N1074A mutation had a more pronounced effect on transport function that is comparable to the mutation of H1 basic residues (**Fig. 2C**). M579 was initially thought to form Van der Waals contacts with the disulfide linkage, but our viability assay results showed that M579A remained viable across all concentrations, indicating that M579 does not coordinate ligand binding events (**Fig. 2C-D**). In contrast to H1, K1077 is the only basic residue found to be within plausible interactive distances with GSSG in the H2 site and forms contact with the glutamyl backbone carboxylate (**Fig. 2B**). Like N1074A, K1077A eliminated the transport activity of Ycf1, leading to cadmium susceptibility (**Fig. 2C**). Finally, the glycyl end of GSSG in the H2 pocket points toward the cytoplasmic opening and has a single hydrogen bond with S575.

Aromatic gating in Ycf1

The GSSG thiol-thiol linkage makes extensive interactions with hydrophobic elements of the bindings site. The disulfide bridge is sandwiched by F576 and W1225 that make Van der Waals contacts (~4Å) with the sulfurs of the bridge (**Fig. 2B**). The F576A and W1225A mutants led to cadmium susceptibility (**Fig. 2C**). F576 in GSSG-Ycf1 shares the same rotamer form as its structural homolog, F594, in MRP1 (**Fig. 3A**). Compared to apo, F576 in GSSG-Ycf1 shifted ~1Å closer towards the center of the pocket cavity, increasing the strength of the Van der Waals contacts with the ligand (**Fig. 3B**). However, in dephos-Ycf1, F576 is rotated by ~96Å towards TM12 and forms hydrophobic interactions with A901 and L904 of the localized R-domain. In this way, F576A has a dual role in both substrate recognition for detoxification purposes and phosphoregulatory responses. Similarlu, W1225 has the same rotamer positioning as its structural homolog, W1245, in MRP1 (**Fig. 3A**). However, compared to its apo state, W1225 of GSSG-Ycf1 is rotated by ~77Å at its γ-carbon position towards NBD1 to flatten its indole ring against the disulfide of GSSG (**Fig. 3B**). Identically, W1225 in dephos-Ycf1 holds the same rotamer, but instead of a hydrophobic interaction it forms a cation-π with R906 instead (**Fig. 3C**). These findings suggest that the aromatic residues are responsible for recognition of binding pocket occupancy that confers to substrate binding affinity.

Discussion

The vacuolar transporter Ycf1 plays a vital role in conferring metal resistance in *S. cerevisiae* and recycling of the glutathione pool by recognizing glutathione in multiple forms: its oxidized form (GSSG), reduced form (GSH), or conjugated to a wide variety of metals with various stoichiometries (GS_2(Cd), GS_2(Pd), GS_2(Hg), GS_3(As)). Our novel substrate-bound structure reveals a potential mechanism by which the transporter can accommodate this variety of substrates that involves more extensive discrimination of the substrate at the H1 site and hydrophobic pocket while leaving a large cavity in the H2 site to accommodate substrates of different sizes (**Fig. 4**). While all four ionic interactions in H1 are essential for substrate recognition, the only critical interactions in H2 are N1074 and K1077, which would presumably allow for a variety of different interactions based on ligand size given different rotamers.

Several binding modes have been identified in yeast and plant mitochondrial glutathione transporters, and GSSG binding in Ycf1 most closely resembles that of the yeast mitochondrial inner membrane transporter Atm1 bound to GSH. There, GSH forms contacts in a highly basic pocket and interestingly, GSH binds to the equivalent of the H1 site. On the other hand, the plant mitochondrial transporter ATM3, which is a homodimer and thus has two equivalent halves, displays a perfectly symmetrical binding to both halves of GSSG, contrasting the biased binding mode of Ycf1 (35). Furthermore, the asymmetric ligand binding of GSSG-Ycf1 has been observed in certain ABC transporters where a single binding pocket can accommodate two of the same substrates in a manner like the two identical halves of GSSG. The bacterial multidrug transporter BmrCD, which has one nonfunctional ATPase domain similarly to Ycf1, binds to the substrate Hoechst 33342 in

an antiparallel fashion (36). The human P-glycoprotein binding to two molecules of zosquidar that also adopt an antiparallel conformation (37). A common theme across these transporters is that their binding pocket often shows predominant binding to one half of the transporter that the biased H1 binding of GSSG-Ycf1 imitates. Further investigation into the antisymmetric ligand conformation could provide invaluable insights into the binding mechanism of ABC transporters.

Pleotropic transporters like *C. albicans* Resistance 1 (CDR1) or Pleotropic resistance protein (PDR5) have a diverse class of substrates. These proteins accomplish promiscuity using multiple binding sites (38-41). In contrast, transporters like Ycf1, which lack multiple binding sites, require an alternative mechanism to be able to transport a wide range of substrates. To accomplish this, Ycf1 has a generally electropositive pocket on the periphery that recognizes GSH moiety, a hydrophobic sandwich located near the thiol moiety to preserve substrate affinity, and a spacious pocket opposite the substrate recognition site to accommodate varying substrate size (**Fig. 4**). Moreover, flexibility within the substrate pocket of Ycf1 is critically important, especially when considering the varying conformations of different metal complexes. The pH of the cytoplasmic space can range from 3.0 – 7.0 in yeast, resulting in different protonation states of GSH (42). In the case of cadmium alone, different GSH-conjugated complexes can form depending on the charge state of cadmium and pH (6.4 vs 7.2) (43). Our GSSG-Ycf1 structure most closely resembles that of Ycf1 at pH 7.2 with a neutral cadmium, which would agree with our flex model in that the metal ion would extend the glutathione on both ends of the complex by ~2Å. In this way, Ycf1 remains a specific transporter for GSH adducted molecules with strong affinity while having the flexibility to transport different complexes.

The overall conformation of GSSG-Ycf1 also differs compared to some glutathione bound transporters. In contrast to Ycf1, which retains a wide pocket, transporters like MRP1 and TAP adopt a narrower, inward-facing conformation as the binding signals for the NBDs to dimerize to occlude the binding pocket and initiate ATP catalysis for substrate turnover (32, 44). In contrast, recent structures of MRP4 bound to varying substrates, most notably PGE2, were found to share the same degree of NBDs positioning as the apo form when in a lipid nanodisc but the opposite when in detergent (45, 46). Nevertheless, in each case, the substrate binds to one half of the transporter more extensively than the other.

Collectively, our study offers key structural details on the substrate recognition mechanism of Ycf1. The discovery of a novel substrate-bound state reveals the molecular constituents responsible for the specific yet diverse transport function of Ycf1. Such insight is potentially promising for future applications of Ycf1 in bioremediation.

Materials and Methods

Cloning, expression, and purification

Codon-optimized *S. cerevisiae* YCF1 gene with N-terminal Flag (DYDDDDK) and C-terminal histidine (10x His) was cloned into the p423_GAL1 yeast expression vector. Binding pocket mutants were generated by site-directed mutagenesis using primers from Millipore sigma and sequenced (Elim Biopharmaceuticals, Inc.) for verification. Ycf1 was expressed as previously described (33). Briefly, p423_GAL1 was transformed into *S. cerevisiae* strain DSY5 and plated onto SC-His (0.67% w/v yeast nitrogen base, 2% w/v glucose, and 0.08% w/v amino acid mix with L-histidine dropout) agar (47). Plates were incubated for 48 hours at 30°C, then single colonies were grown in a 50mL SC-His primary culture for 24 hours at 30°C. Secondary cultures containing 750mL SC-His media were inoculated with 2% of the primary culture and grown for an additional 24 hours under the same condition, then 250 mL YPG (1% w/v yeast extract, 1.5% w/v peptone, and 2% w/v galactose) media was used to induce for Ycf1 expression and grown for 16 hours at the same temperature. Cells were harvested by centrifugation at 5000g for 30min at 4°C and pellets were frozen at -80°C for crude membrane preparation.

Ycf1 purification was conducted as previously described with a slight modification in detergents (35). Briefly, harvested cell pellets were resuspended in cold lysis buffer (50mM Tris-Cl, 300mM NaCl, 2.5µM aprotinin, 2.5µM pepstatin, 6.25µM leupeptin, and 0.5mg/mL 4-benzenesulfonyl fluoride hydrochloride, pH 7.0) at a 3.2 mL/g of cell pellet ratio. Cell lysis was conducted using a bead beater with 0.5mm glass beads for 8 cycles with 45s on and 5 min off in between cycles. Lysates were vacuum filtered through a coffee filter and membranes were harvested by ultracentrifugation at 112,967x*g* for 1.5 hours. Crude membranes were stored at -80ºC for purification. Overnight solubilization of membranes was conducted using the same lysis buffer as described above with the addition of 0.5% 2,2-didecylpropane-1,3-bis-β-D-maltopyranoside (LMNG)/0.05% cholesteryl hemisuccinate (CHS) at a 15mL/g of membrane ratio. Membranes were clarified by ultracentrifugation at 34155x*g* for 30min at 4ºC, and the resulting supernatant was filtered through a 0.4µm filter. Ni-NTA immobilized metal affinity chromatography (IMAC) column and size exclusion chromatography (SEC) were performed exactly as described in Khandelwal, et al. with a modification of detergent using an additional 0.02% glycol-diosgenin.

Cryo-EM grid preparation and data acquisition.
Size exclusion purified protein was quantified with BCA assay (Pierce), then concentrated Ycf1 (2.5 mg/mL) was incubated in ice-cold 10mM GSSG for one hour. Following this, 5uL of sample was applied to a glow discharged QF-R2/1 Cu 200M grid (Electron Microscopy Sciences). Grids were frozen into -185ºC liquid ethane using a Leica EM GP2 automatic plunge freezer equilibrated to 80% humidity and 10ºC with a 10s sample incubation time and a 2.5s blot time on Whatman 1 paper. Sample acquisition was conducted at the Pacific Northwest Center for Cryo-EM on a Titan Krios transmission electron microscope (Gatan K3 summit detector + Biocontinuum gif 20EV slit) with a defocus of 2.7µm pixel size of 0.6483Å/pix. A total of 15606 movies were collected at an exposure time of 1.09s with 65 frames per exposure, averaging to a total frame exposure dose to be ~48e^-/Å.

Cryo-EM data processing.
The collected dataset was processed using CryoSPARC version 4.2.1. Movies were imported into CryoSPARC and patch motion corrected followed by contrast transfer function (CTF) estimation. The automatic blob picking function was used to obtain 5,593,679 particles that were further curated by the interactive inspect pick function to generate a total of 1,827,672 particles extracted to 2.736Å/pixel with a box size of 400 pixel. Three rounds of reference-free 2D classification were performed to obtain 515,916 particles for template re-picking. Another three rounds of 2D classifications were conducted on template picked particles, resulting in 918,339 particles for *ab-initio* reconstruction. Using the *ab-initio* 3D map as reference, hetero refinement was conducted to generate six classes. Three classes with continuous density were selected for non-uniform (NU) refinement. Two classes with representative morphology of Ycf1 and continuous density were combined and re-extracted to 0.684Å/pixel with a box size of 440 pixel for another round of NU-refinement, yielding a 3.32Å 3D map. Particle curation was performed to only select for particles with CTF estimation of 4Å or better. Iterative rounds of NU-refinement and CTF refinement were conducted to obtain a map of 3.15Å. The final resolution of map was improved by using a manual mask with local refinement that resulted in a 3.14Å map with 191,581 particles.

Model building and refinement.
The previously established inward-facing wide apo structure of Ycf1 (PDBID:7M69) was used as the initial model (33). Model building was conducted using the ISOLDE (version 1.3) plugin in ChimeraX with minor manual fitting conducted with COOT (48-50). Iterative rounds of real-space refinement in Phenix were used to improve model quality. Final model with statistics reported against the CryoSPARC generated map. Figures preparation was done using UCSF ChimeraX and ligand binding analysis was done using Ligplot (51).

Ycf1 mutant expression in *S. cerevisiae* and yeast cadmium susceptibility assay.

To express Ycf1 and mutants for the cadmium susceptibility assay, *S. cerevisiae* strain BY4742 with endogenous Ycf1 knockout (Horizon Discovery) were transformed following the Frozen-EZ Yeast Transformation II protocol (Zymo Research). Transformed yeast strains were grown for 48 hours on YNB-His agar plates at 30°C. Individual colonies were picked and diluted to approximately 0.2 OD_{600} using sterile reagent, ACS grade H_2O (Midland Scientific) that was further filtered with a 0.22µm syringe filter. Cells were then spotted onto YRG (yeast nitrogen base with ammonium sulfate 0.67% w/v, raffinose 1% w/v, galactose 2% w/v, CSM-His 0.077% w/v and 2% w/v agar) agar plates with and without 100 µM $CdCl_2$ using a replica plater for 96 well plate (Sigma-Aldrich). Images were collected following 5 days of incubation at 30 °C with a Bio-Rad Chemidoc MP Imaging System (Bio-Rad). Quantification of spots were analyzed using the ImageJ software (52).

Acknowledgments

This research was supported by grants from the National Institute of Allergy and Infectious Disease (NIH R01 AI156270 (TMT)). Micrograph collection was performed at the Pacific Northwest Center for Cryo-EM (PNCC). A special thank you to Nancy Meyer for assisting with data acquisition along with the staff of PNCC.

References

1. C. Thomas, R. Tampé, Multifaceted structures and mechanisms of ABC transport systems in health and disease. *Current Opinion in Structural Biology* **51**, 116-128 (2018).
2. M. M. Gottesman, S. V. Ambudkar, Overview: ABC Transporters and Human Disease. *Journal of Bioenergetics and Biomembranes* **33**, 453-458 (2001).
3. J. A. Lemire, J. J. Harrison, R. J. Turner, Antimicrobial activity of metals: mechanisms, molecular targets and applications. *Nature Reviews Microbiology* **11**, 371-384 (2013).
4. M. Balali-Mood, K. Naseri, Z. Tahergorabi, M. R. Khazdair, M. Sadeghi, Toxic Mechanisms of Five Heavy Metals: Mercury, Lead, Chromium, Cadmium, and Arsenic. *Front Pharmacol* **12**, 643972 (2021).
5. C. R. Kothapalli, Differential impact of heavy metals on neurotoxicity during development and in aging central nervous system. *Current Opinion in Toxicology* **26**, 33-38 (2021).
6. M. Jozefczak, T. Remans, J. Vangronsveld, A. Cuypers, Glutathione is a key player in metal-induced oxidative stress defenses. *Int J Mol Sci* **13**, 3145-3175 (2012).
7. M. J. Penninckx, An overview on glutathione in Saccharomyces versus non-conventional yeasts. *FEMS Yeast Research* **2**, 295-305 (2002).
8. A. Potęga, Glutathione-Mediated Conjugation of Anticancer Drugs: An Overview of Reaction Mechanisms and Biological Significance for Drug Detoxification and Bioactivation. *Molecules* **27** (2022).
9. M. E. Sears, Chelation: harnessing and enhancing heavy metal detoxification--a review. *ScientificWorldJournal* **2013**, 219840 (2013).
10. A. M. A. Mazari *et al.*, The Multifaceted Role of Glutathione S-Transferases in Health and Disease. *Biomolecules* **13** (2023).
11. P. B. Tchounwou, C. G. Yedjou, A. K. Patlolla, D. J. Sutton, Heavy metal toxicity and the environment. *Exp Suppl* **101**, 133-164 (2012).
12. L. Järup, Hazards of heavy metal contamination. *British Medical Bulletin* **68**, 167-182 (2003).

13. N. Ballatori, S. M. Krance, R. Marchan, C. L. Hammond, Plasma membrane glutathione transporters and their roles in cell physiology and pathophysiology. *Mol Aspects Med* **30**, 13-28 (2009).
14. P. K. Smitherman, A. J. Townsend, T. E. Kute, C. S. Morrow, Role of multidrug resistance protein 2 (MRP2, ABCC2) in alkylating agent detoxification: MRP2 potentiates glutathione S-transferase A1-1-mediated resistance to chlorambucil cytotoxicity. *J Pharmacol Exp Ther* **308**, 260-267 (2004).
15. M. Bellion, M. Courbot, C. Jacob, D. Blaudez, M. Chalot, Extracellular and cellular mechanisms sustaining metal tolerance in ectomycorrhizal fungi. *FEMS Microbiology Letters* **254**, 173-181 (2006).
16. G. Noctor, A. Mhamdi, G. Queval, C. H. Foyer, Regulating the Redox Gatekeeper: Vacuolar Sequestration Puts Glutathione Disulfide in Its Place *Plant Physiology* **163**, 665-671 (2013).
17. S. A. Pearson, J. A. Cowan, Glutathione-coordinated metal complexes as substrates for cellular transporters. *Metallomics* **13** (2021).
18. K. R. Parzych, D. J. Klionsky, Vacuolar hydrolysis and efflux: current knowledge and unanswered questions. *Autophagy* **15**, 212-227 (2019).
19. J. A. Wemmie, M. S. Szczypka, D. J. Thiele, W. S. Moye-Rowley, Cadmium tolerance mediated by the yeast AP-1 protein requires the presence of an ATP-binding cassette transporter-encoding gene, YCF1. *J Biol Chem* **269**, 32592-32597 (1994).
20. Z. S. Li, M. Szczypka, Y. P. Lu, D. J. Thiele, P. A. Rea, The yeast cadmium factor protein (YCF1) is a vacuolar glutathione S-conjugate pump. *J Biol Chem* **271**, 6509-6517 (1996).
21. Z. S. Li *et al.*, A new pathway for vacuolar cadmium sequestration in Saccharomyces cerevisiae: YCF1-catalyzed transport of bis(glutathionato)cadmium. *Proc Natl Acad Sci U S A* **94**, 42-47 (1997).
22. O. Gueldry *et al.*, Ycf1p-dependent Hg(II) detoxification in Saccharomyces cerevisiae. *Eur J Biochem* **270**, 2486-2496 (2003).
23. Z. Nagy *et al.*, Role of the yeast ABC transporter Yor1p in cadmium detoxification. *Biochimie* **88**, 1665-1671 (2006).
24. S. R. Talemi *et al.*, Mathematical modelling of arsenic transport, distribution and detoxification processes in yeast. *Mol Microbiol* **92**, 1343-1356 (2014).
25. R. Wysocki, M. J. Tamás, How Saccharomyces cerevisiae copes with toxic metals and metalloids. *FEMS Microbiol Rev* **34**, 925-951 (2010).
26. D. Shim *et al.*, Transgenic poplar trees expressing yeast cadmium factor 1 exhibit the characteristics necessary for the phytoremediation of mine tailing soil. *Chemosphere* **90**, 1478-1486 (2013).
27. B. Morgan *et al.*, Multiple glutathione disulfide removal pathways mediate cytosolic redox homeostasis. *Nature Chemical Biology* **9**, 119-125 (2013).
28. S. P. C. Cole, Targeting Multidrug Resistance Protein 1 (MRP1, ABCC1): Past, Present, and Future. *Annual Review of Pharmacology and Toxicology* **54**, 95-117 (2014).
29. S. H. Lee, G. A. Altenberg, Expression of functional multidrug-resistance protein 1 in Saccharomyces cerevisiae: effects of N- and C-terminal affinity tags. *Biochemical and Biophysical Research Communications* **306**, 644-649 (2003).
30. X.-Q. Ren *et al.*, Functional Comparison between YCF1 and MRP1 Expressed in Sf21 Insect Cells. *Biochemical and Biophysical Research Communications* **270**, 608-615 (2000).

31. R. Tommasini *et al.*, The human multidrug resistance-associated protein functionally complements the yeast cadmium resistance factor 1. *Proc Natl Acad Sci U S A* **93**, 6743-6748 (1996).
32. Z. L. Johnson, J. Chen, Structural Basis of Substrate Recognition by the Multidrug Resistance Protein MRP1. *Cell* **168**, 1075-1085.e1079 (2017).
33. N. K. Khandelwal *et al.*, The structural basis for regulation of the glutathione transporter Ycf1 by regulatory domain phosphorylation. *Nature Communications* **13**, 1278 (2022).
34. K. Nitesh Kumar, M. T. Thomas, Structural Basis for Autoinhibition by the Dephosphorylated Regulatory Domain of Ycf1. *bioRxiv* 10.1101/2023.06.22.546176, 2023.2006.2022.546176 (2023).
35. C. Fan, D. C. Rees, Glutathione binding to the plant AtAtm3 transporter and implications for the conformational coupling of ABC transporters. *eLife* **11**, e76140 (2022).
36. T. M. Thaker *et al.*, Asymmetric drug binding in an ATP-loaded inward-facing state of an ABC transporter. *Nature Chemical Biology* **18**, 226-235 (2022).
37. A. Alam *et al.*, Structure of a zosuquidar and UIC2-bound human-mouse chimeric ABCB1. *Proc Natl Acad Sci U S A* **115**, E1973-e1982 (2018).
38. J. Ahmed, II, A. A. Abdul Hamid, K. B. Abd Halim, A. T. Che Has, P-glycoprotein: new insights into structure, physiological function, regulation and alterations in disease. *Heliyon* **8**, e09777 (2022).
39. A. Harris *et al.*, Structure and efflux mechanism of the yeast pleiotropic drug resistance transporter Pdr5. *Nature Communications* **12**, 5254 (2021).
40. Y. Lee, E. Puumala, N. Robbins, L. E. Cowen, Antifungal Drug Resistance: Molecular Mechanisms in Candida albicans and Beyond. *Chem Rev* **121**, 3390-3411 (2021).
41. M. K. Rawal *et al.*, Newly identified motifs in Candida albicans Cdr1 protein nucleotide binding domains are pleiotropic drug resistance subfamily-specific and functionally asymmetric. *Scientific Reports* **6**, 27132 (2016).
42. M. Valli *et al.*, Intracellular pH distribution in Saccharomyces cerevisiae cell populations, analyzed by flow cytometry. *Appl Environ Microbiol* **71**, 1515-1521 (2005).
43. O. Delalande *et al.*, Cadmium – glutathione solution structures provide new insights into heavy metal detoxification. *The FEBS Journal* **277**, 5086-5096 (2010).
44. L. James, L. O. Michael, M. Victor, C. Jue, The principles of peptide selection by the transporter associated with antigen processing. *bioRxiv* 10.1101/2023.06.16.545308, 2023.2006.2016.545308 (2023).
45. S. Pourmal *et al.*, Structural basis of prostaglandin efflux by MRP4. *Nature Structural & Molecular Biology* 10.1038/s41594-023-01176-4 (2024).
46. M. Bloch, I. Raj, T. Pape, N. M. I. Taylor, Structural and mechanistic basis of substrate transport by the multidrug transporter MRP4. *Structure* **31**, 1407-1418.e1406 (2023).
47. M. V. Dilworth *et al.*, Microbial expression systems for membrane proteins. *Methods* **147**, 3-39 (2018).
48. T. Croll, ISOLDE: a physically realistic environment for model building into low-resolution electron-density maps. *Acta Crystallographica Section D* **74**, 519-530 (2018).
49. P. Emsley, K. Cowtan, Coot: model-building tools for molecular graphics. *Acta Crystallogr D Biol Crystallogr* **60**, 2126-2132 (2004).
50. E. F. Pettersen *et al.*, UCSF ChimeraX: Structure visualization for researchers, educators, and developers. *Protein Sci* **30**, 70-82 (2021).

51. R. A. Laskowski, M. B. Swindells, LigPlot+: Multiple Ligand–Protein Interaction Diagrams for Drug Discovery. *Journal of Chemical Information and Modeling* **51**, 2778-2786 (2011).
52. A. A. Petropavlovskiy, M. G. Tauro, P. Lajoie, M. L. Duennwald, A Quantitative Imaging-Based Protocol for Yeast Growth and Survival on Agar Plates. *STAR Protocols* **1**, 100182 (2020).

Figures and Tables

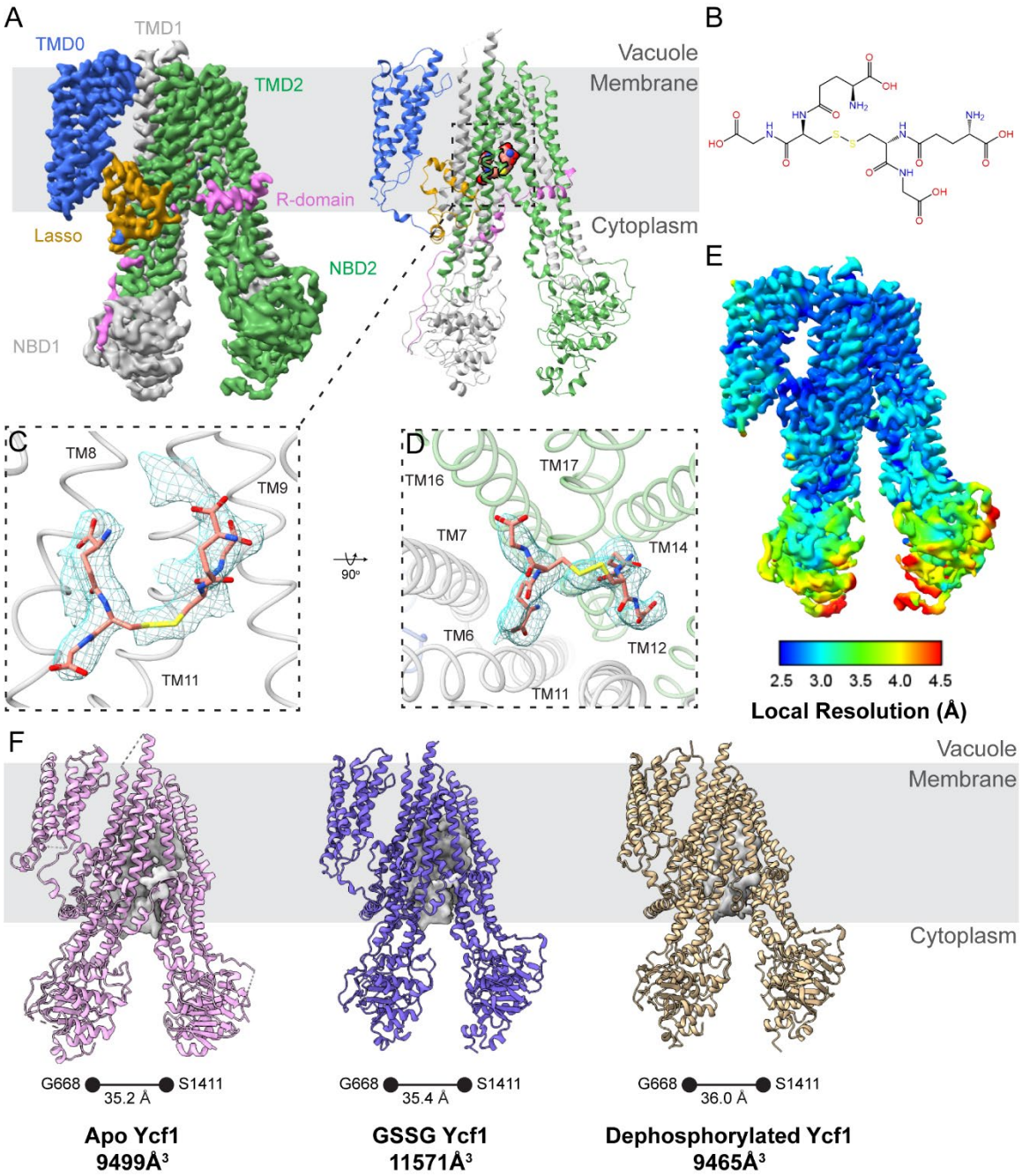

Figure 1. *Overview of cryo-EM map and model. (A) Density map and cartoon model of GSSG-bound Ycf1 showing the transmembrane domain 0 (TMD0, blue), transmembrane domain 1 (TMD1, gray), transmembrane domain 2 (TMD2, green), nucleotide binding domain 1 (NBD1, gray), nucleotide binding domain 2 (NBD2, green), lasso motif (gold), and the regulatory domain (R-domain, magenta). (B) Two-dimensional representation of GSSG. (C) Frontal slice of model showing GSSG and its corresponding density with nearby TM helices. (D) A 90-degree rotated view of (C) from the NBDs up into pocket cavity. (E) Local resolution of cryo-EM map with rainbow coloring scheme (F) Substrate cavity and NBDs width comparison between apo (PDBID:7M69, pink), GSSG-bound (blue), and dephosphorylated (PDBID: 8SG4, wheat) of Ycf1.*

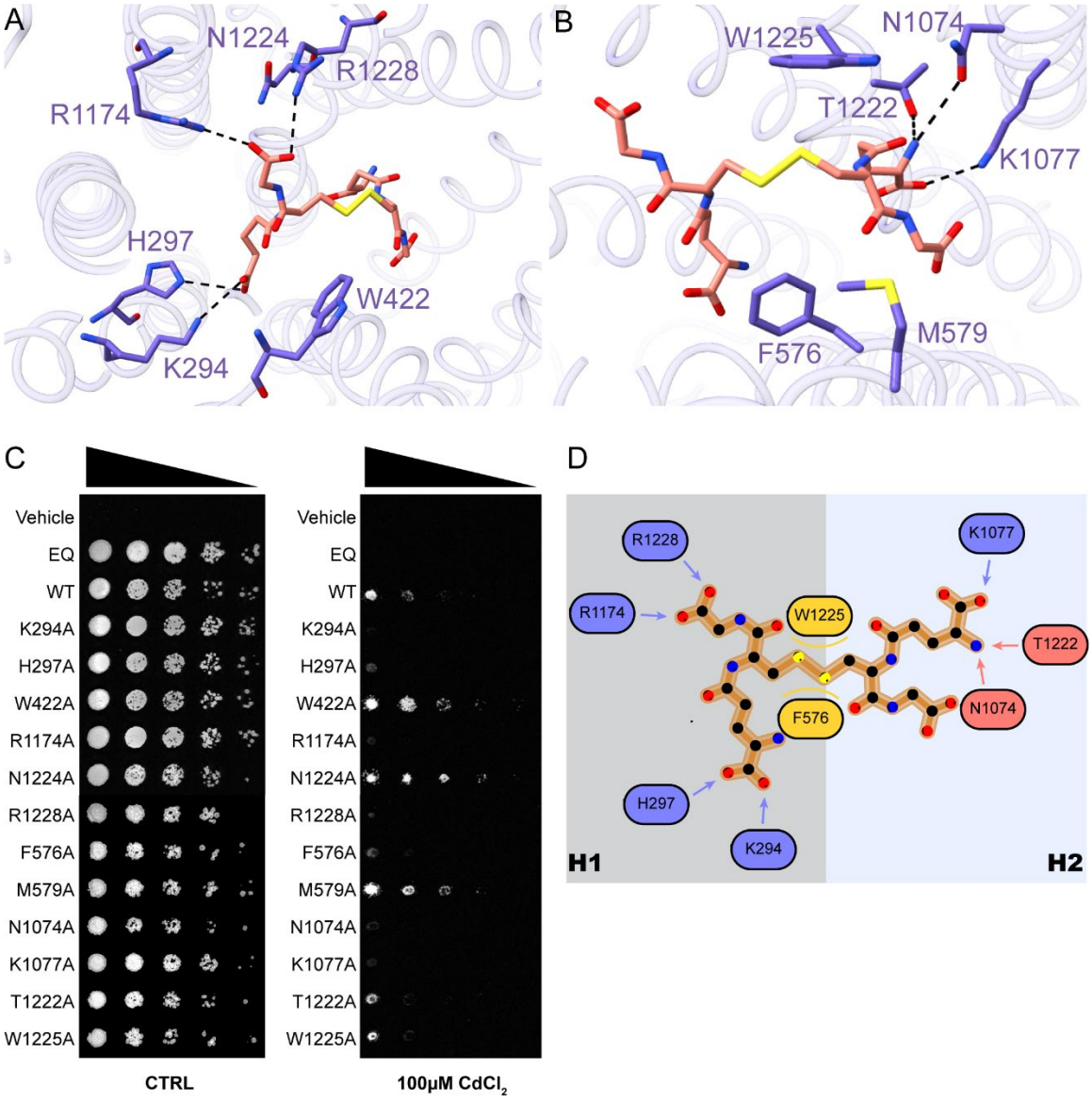

Figure 2. *Molecular determinants of substrate recognition in Ycf1. (A) H1 pocket residues with ionic and hydrogen bonds shown with dashed lines. (B) H2 pocket residues with ionic and hydrogen bonds shown with dashed lines. (C) Yeast cadmium assay shown mutant viability under 100μM cadmium chloride growth conditions. (D) Overall schematic of GSSG binding interactions with charged interactions (blue), hydrogen bonds (red), and hydrophobic interactions (yellow) shown.*

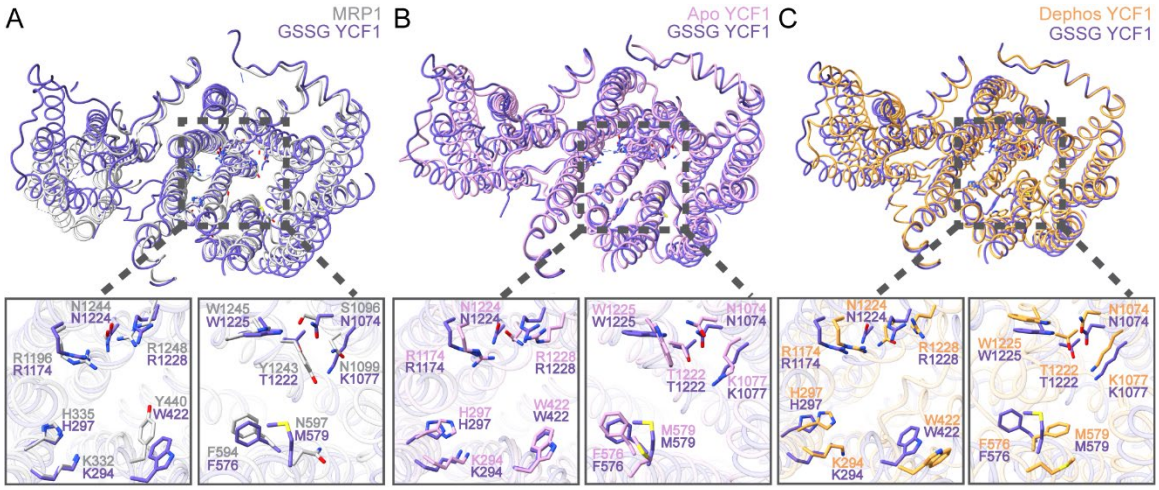

Figure 3. *Binding pocket residue positioning comparison. (A-C) LTC4-bound Mrp1 (Grey), Apo Ycf1 (Pink), and Dephosphorylated Ycf1 (orange) overlaid with GSSG-bound Ycf1 (blue) viewed from NBDs into binding cavity to reveal H1 and H2 site residues.*

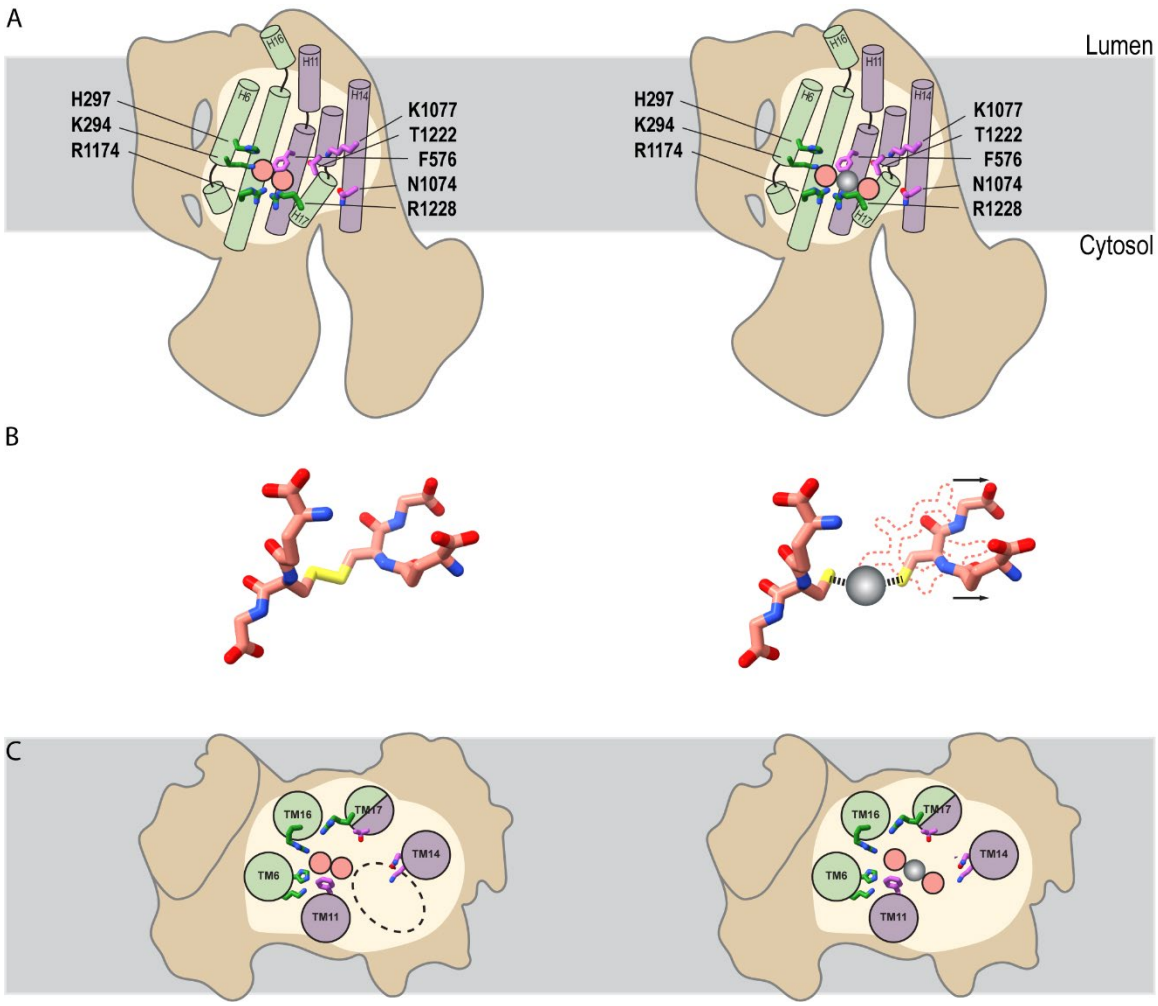

Figure 4. *Proposed model for flexible binding pocket. (A) Front view of GSSG (pink spheres) and metal (silver sphere) interactions with H1 and H2 pocket residues. (B) Representative of changes in GSSG conformation in the presence of a metal conjugation. (C) NBD view of GSSG and metal interactions with H and H2 pocket residues.*